AIAA

AIAA 2000-0409

Dynamics of Active Separation Control at High Reynolds Numbers

LaTunia G. Pack and Avi Seifert

NASA Langley Research Center

Hampton, VA

38th AIAA Aerospace Sciences Meeting and Exhibit
January 10-13, 2000/ Reno, NV

Dynamics of Active Separation Control at High Reynolds Numbers

LaTunia G. Pack[†] and Avi Seifert[*]
NASA Langley Research Center, Hampton, VA

Abstract

A series of active flow control experiments were recently conducted at high Reynolds numbers on a generic separated configuration. The model simulates the upper surface of a 20% thick Glauert-Goldschmied type airfoil at zero angle of attack. The flow is fully turbulent since the tunnel sidewall boundary layer flows over the model. The main motivation for the experiments is to generate a comprehensive data base for validation of unsteady numerical simulation as a first step in the development of a CFD design tool, without which it would not be possible to effectively utilize the great potential of unsteady flow control. This paper focuses on the dynamics of several key features of the baseline as well as the controlled flow.

It was found that the thickness of the upstream boundary layer has a negligible effect on the flow dynamics. It is speculated that separation is caused mainly by the highly convex surface while viscous effects are less important. The two-dimensional separated flow contains unsteady waves centered on a reduced frequency of 0.8, while in the three dimensional separated flow, frequencies around a reduced frequency of 0.3 and 1 are active. Several scenarios of resonant wave interaction take place at the separated shear-layer and in the pressure recovery region. The unstable reduced frequency bands for periodic excitation are centered on 1.5 and 5, but these reduced frequencies are based on the length of the baseline bubble that shortens due to the excitation. The conventional swept wing-scaling works well for the coherent wave features.

Reproduction of these dynamic effects by a numerical simulation would provide benchmark validation.

Nomenclature

c_μ steady blowing momentum coefficient, $\equiv J/cq$

$<c_\mu>$ oscillatory blowing momentum coefficient, $\equiv <J'>/cq$

C_μ combined blowing momentum coefficient, $\equiv (c_\mu; <c_\mu>)$

c model chord

C_p wall pressure coefficient, $\equiv (P - P_S)/q$

f oscillation frequency [Hz]

F^+ reduced frequency, $\equiv f * X_{sp}/U_\infty$

F fundamental excitation frequency

h slot height or width

H height of separated region

J momentum at slot exit, $\equiv \rho h U_j^2$

M Mach number

nF integer multiple of the excitation freq

P pressure

q free stream dynamic pressure, $q = 1/2\rho U_\infty^2$

R reattachment

R_c chord Reynolds number, $R_c = U_\infty c/v$

S separation

T temperature

U, u average and fluctuating streamwise velocity

U_ϕ phase velocity

x/c normalized streamwise location

X_{sp} distance from actuator or separation to reattachment

z spanwise location

Λ sweep angle [deg]

v kinematic viscosity

ρ density

θ BL momentum thickness

Abbreviations

BL   boundary layer

LE   leading edge

TE   trailing edge

$<>$ phase locked values

Subscripts

b   baseline parameters

c   cavity

f   related to excitation frequency

j   conditions at blowing slot

e   conditions at BL edge

∞ free-stream conditions

2D   two-dimensional

3D   three-dimensional

Superscripts

$'$ root mean square of fluctuating value

---

† Research Engineer, Flow Physics and Control Branch, member of AIAA.
* Senior lecturer, Dep. of Fluid Mech. & Heat transfer, Faculty of Eng, Tel-Aviv University, Ramat Aviv 69978, Israel, member AIAA.

1. Introduction

This paper is the third in a series of publications describing experiments that were aimed at improving our understanding of controlling separated flows at flight Reynolds numbers and providing a comprehensive database for validation of unsteady CFD design tools. Specifically, effects of the upstream boundary layer thickness, compressibility, sweep and location for introduction of the control input are explored. A previous publication[1] presented some of the experimental results for incompressible 2D flow over the same model. Periodic excitation is the primary control mechanism, but steady mass transfer is also used, for comparison of effectiveness and also in order to provide fully attached steady flow, since the baseline uncontrolled flow contains a large turbulent separation bubble.

The model simulates the upper surface of a 20% thick Glauert-Goldschmied type airfoil and has some features in common with a backwards-facing step with the exception that the flow on the model can be fully re-attached with effective control. Without control, the flow separates at the highly convex region of the model (x/c=0.65, Fig. 1) and a large turbulent separation bubble is formed. Periodic excitation is applied from the slot located at x/c=0.64 or at x/c=0.59 to gradually eliminate the separation bubble. The effects of steady suction or blowing were also tested. The dynamics of these steady flow control methods are compared to those of the periodic excitation.

A brief summary of the incompressible 2D findings that were presented in Ref. 1 is repeated here for completeness. The baseline flow was carefully documented and found to be weakly dependent on Reynolds number. The baseline flow is fully turbulent so laminar-turbulent transition, due to the active separation control, does not effect the data trends. The thickness of the upstream boundary layer was monitored and controlled. A reduction of about 40% in the boundary layer momentum thickness had only a minor effect on the baseline separation and its control. The spanwise uniformity of the wall pressure distribution was found to be very good and improved as the separation was controlled. The baseline reattachment point was found to be about one separation height downstream of the peak in the wall pressure fluctuations. The separation height is taken as the model elevation at separation (i.e. x/c=0.65, H=0.115c). The level of this peak increased as reattachment moved forward due to control, regardless of the control method. Steady suction or blowing with a momentum coefficient of 2-4% is required to fully reattach the flow to the model surface and recover the ideal pressure distribution. Active control using periodic excitation is comparable to steady suction and significantly more effective than steady blowing. Periodic excitation is capable of reattaching the flow

but is not capable of reproducing the same pressure jump across a slot as suction does. This is presumably since the periodic excitation relies on enhanced mixing that is by nature a convective phenomena rather than a local one that is generated by the severe suction. It was found that the superposition of weak suction on the oscillatory excitation significantly enhances the receptivity of the separated shear layer to the fundamental excitation frequency. Detailed dynamics of the wall pressure fluctuations that explain some of the observed features will be discussed.

The measurement tools used for the dynamic testing are 12 dynamic pressure transducers that are positioned next to the static pressure taps (x symbols on Fig. 2). The dynamic pressure measurement allows the evaluation of random and coherent pressure waves. In addition, the measurement of the cavity pressure fluctuations provides an opportunity for a comprehensive description of the control input.

The dynamics of pressure fluctuations measured over a wide range of separated flow configurations were reviewed in Reference 2. It was shown that the level of pressure fluctuations increase downstream of separation, and peaks close to and upstream of reattachment, at values of 4-10% the dynamic pressure. The dimensionless dominant frequency, based on the length of the separated region and on the free stream velocity was between 0.5 and 0.8. The excellent review of impinging shear-layers by Rockwell[3], supports the above findings and discusses linear as well as non-linear evolution of the separated and reattached shear layer.

Two extensive direct numerical simulations (DNS) of separated flow were recently published[4,5]. For a backwards-facing step, the separated free shear-layer was unsteady with a dominant range of F^+ of one at separation and it reduced to 0.5 at reattachment. The reduction in F^+ was an indication of dissipation of the small structures or vortex merging. The F^+ was based on the length of the bubble, $X_{sp}\sim6.3$ step heights. The phase speed of the $F^+=0.5$ structures increased downstream of reattachment. The calculated wall pressure fluctuations peaked just upstream of reattachment, with a value lower than experimentally measured. The second DNS[5] deals with separated and re-attached flow due to an adverse pressure gradient imposed on a flat plate boundary layer. The main difference between this flow and the backwards-facing step is the lack of a fixed separation point, that indeed was found to fluctuate significantly in the streamwise direction. The dominant F^+ as well as the peak of C_p' at reattachment were similar in both flows.

This paper does not pretend to provide a comprehensive description of the flow field dynamics, as this could not be provided using only the wall pressures. Rather it attempts to deepen the understanding of several key features and provide

validation cases for future CFD. A brief review of the experimental set-up is provided in Sec. 2. The 2D baseline flow is discussed in Sec. 3. The effect of the upstream BL thickness is discussed in Sec. 3.2. The effect of sweep on the baseline flow spectra is discussed in Sec. 3.3. The remainder of the paper deals with the controlled flow. Sec. 4.1 describes the effects of the excitation frequency and its amplitude. The effects of sweep on the 3D controlled flow are discussed in Sec. 4.2. Finally, the unsteady effects of weak steady suction and periodic excitation are compared in Sec. 4.3.

2. Description of the Experiment

2.1 Overview
This section contains a brief description of the experiment. A more detailed description can be found in References 1 and 6.

2.2 Model
The 200 mm chord model simulates the upper surface of a 20% thick airfoil that is a variation on the Glauert Glas II airfoil[7]. A moderate favorable pressure gradient up to 55% of the chord is followed by a severe adverse pressure gradient, imposed by the highly convex surface at x/c~0.6, that relaxes towards the trailing edge (see Fig. 1). The model was mounted on the sidewall of the tunnel and therefore the flow over the model was fully turbulent. Two alternative excitation slot locations, x/c=0.59 and x/c=0.64, were available. The slots were about 0.25% chord wide (0.50 mm ±20%), and allowed an almost tangential downstream introduction of momentum (the slots are inclined at 30° to the surface because of manufacturing considerations, see Fig. 1). The model design also enabled testing at two sweep angles, Λ=0 degrees and Λ=30 degrees. A top view of the 2D configuration is shown in Fig. 2. The symbols in Fig. 2 show the distribution of the static pressure taps and dynamic pressure transducers, while the vertical thick lines mark the location of the end plates that isolate the boundary layers on the floor and ceiling of the wind tunnel from affecting the flow over the model. Ten dynamic pressure transducers (marked by x symbols on Fig. 2) are installed under the model surface, inside small volume cavities. The cavities are connected to the surface of the model by tiny orifices, 0.254 mm in diameter. The effect of this installation on the frequency response of the dynamic pressure transducers was studied using a comprehensive bench-top calibration and occasional in-situ testing by a Piezo-electric actuator. In addition, a transducer was flush mounted near the trailing edge of the turntable (x/c=1.4) next to a recessed pressure transducer and their readings are compared. The full scale of the dynamic pressure transducers is 10 psid. They are referenced to the static wall pressures immediately next to the orifice locations or to the wind tunnel plenum pressure in order to maintain optimal resolution even at static pressures that exceed the transducer's range. One dynamic pressure transducer is also installed inside the model cavity, midway between the end plates and about 30-mm from the slot exit. It is used to monitor the cavity pressure oscillations and to correlate the wind tunnel experiments with the bench-top tests that were conducted in order to correlate the slot exit velocities with the cavity pressure oscillations[1].

2.3 Oscillatory Blowing System
The oscillatory blowing system is capable of introducing a wide range of steady and periodic momentum combinations from the cavity inside the model to the external flow. More details can be found in References 1 and 8.

2.4 Boundary Layer Measurement System
The boundary layer probe consisted of a Pitot-probe that was connected to both a static and a dynamic pressure transducer. The probe was mounted to the backside of the model inside a temperature-controlled box. The boundary layer probe penetrated to the flow side of the model through six alternative slots in the turntable. The internal diameter of the probe tip was 0.254mm and when touching the wall, the probe integrated the total pressure from 0.1mm to 0.35mm from the wall. A more detailed description of the boundary layer measurement system can be found in Reference 1.

2.5 Experimental Uncertainty
The experimental uncertainty in the determination of C_p' amplitude was estimated to be ±15%. The uncertainty of the phase of the fundamental excitation frequency and its second harmonic was estimated to be ±10 deg. This leads to an uncertainty of the calculated phase velocities of ±6%. The estimation of the $<c_\mu>$ was within ±25% of the quoted values, but this value is probably lower for most of the non-cryogenic conditions cited in this paper. The steady mass flux momentum coefficients are within ±5% of the cited values or 0.01% absolute value (the bigger of the two). Additional uncertainty information can be found in Refs. 8 and 1.

2.6 Experimental Flow Conditions
The experiments were conducted at Mach numbers from 0.20 to 0.70 and chord Reynolds numbers ranging from 2.4×10^6 to 39×10^6.

3. Dynamics of the Baseline Flow

3.1 Baseline 2D Flow

The Reynolds number has a weak effect on the model pressure distributions, as seen from the 2D data in Fig. 3. Note the C_p' ordinate is on the right side of the figure. The flow separation (at x/c=0.65) is not affected by the presence of the blowing slot, by an interaction between the external flow and the cavity[1], or even by sweeping the model to Λ=30 deg (Fig. 3 here and Fig. 3 of Ref. 6). Mean and fluctuating pressure distributions over a R_c range of 7 to 26x10^6 were compared (Fig. 5, Ref. 1), showing very weak R_c sensitivity. Fig. 3 compares data measured at R_c=2.4x10^6 with data taken at R_c=16x10^6. The very small effect the Reynolds number has on the wall pressure distributions facilitates studying the pressure field dynamics at relatively low R_c (i.e., non-cryogenic temperatures), where the flat range of the installed dynamic pressure transducers' frequency response extends up to 2.5 kHz.

The fluctuating wall pressures (C_p'), also shown in Fig. 3, are very low upstream of separation. A significant increase in C_p' is seen for x/c>0.64 (the thick dashed vertical line indicates the slot location) and a further increase as reattachment is approached (x/c=1.1). Reattachment is assumed to be between the location of $C_{p'max}$ (denoted by x/c($C_{p'max}$)) and one separation height downstream of x/c($C_{p'max}$)[2,4,5]. The separation height is taken as the model elevation at separation (i.e. x/c=0.65, H=0.115c). The wall pressure fluctuations decrease downstream of reattachment as the turbulent boundary layer readjusts to the zero pressure gradient flow. The pressure amplitude spectra at R_c=4.2x10^6 are presented in Fig. 4. Note that the spectra of x/c≥0.85 are shifted up by a decade with respect to previous x/c spectra. Very close to separation (x/c=0.73), a broad band of active frequencies centered on F$^+$=0.8 can be observed to slightly rise above the background random pressure fluctuations. Note that the frequencies were reduced using the length of the separated region (~c/2) and the free stream velocity. These frequencies are probably related to a Kelvin-Helmholz type of instability that is independent of the Reynolds number or to the laminar-turbulent state of the boundary layer prior to separation. The low frequency range fills very quickly above the bubble (x/c=0.85), and the overall pressure fluctuation level increases. A further increase in C_p', accompanied by a halving of the dominant frequencies to F$^+$=0.4, occurs at reattachment (x/c=1.11). The low frequencies decay very rapidly in the attached boundary layer (x/c=1.42), leaving a dominant band of F$^+$ centered on F$^+$=0.5. It is highly probable that sub-harmonic resonance takes place above the bubble, but the resolution of the measurements did not allow a clear identification of the process dynamics. This point will be addressed again in Section 4.1 discussing the controlled flow.

3.2 The Effect of the Upstream Boundary Layer Thickness

It was demonstrated[1] that the thickness of the upstream boundary layer has very little effect on the baseline and controlled pressure distribution in the range R_c=7-26x10^6. Furthermore, it was demonstrated that thinning of the upstream boundary layer by distributed suction upstream of the model by as much as 43% (based on the momentum thickness) does not have a measurable effect on the integral parameters. This point is addressed again here at a lower chord Reynolds number (R_c=4.2x10^6, M=0.25, 2D flow, and x/c=0.64 slot) where the effect is expected to be larger than at high R_c. Fig. 5 shows the mean total pressure profiles measured at 1.25c upstream of the model leading edge. The strong suction reduced the momentum thickness by 35% and the shape factor from 1.29 to 1.17. The Reynolds numbers based on the upstream BL momentum thickness (Re$_\theta$) were 31x10^3 and 20x10^3 for the baseline and boundary layer control (BLC) flows respectively. The corresponding model pressure distributions are presented in Fig. 6. The main effect of the thinner upstream boundary layer is a stronger deceleration of the flow upstream of the LE, in accordance with the ideal flow prediction. The pressure distributions are identical from x/c=0 to separation, x/c=0.65. The thinner boundary layer flow separates at a slightly higher C_p and generates a lower C_p' at x/c=0.67 (right hand ordinate). The pressure recovery downstream of the bubble is similar, but the reattachment C_p is higher for the thinner boundary layer flow. This is accompanied by a higher C_p'. It is speculated that the higher C_p' at reattachment causes the higher C_p that is measured downstream of reattachment, due to the impingement of the large coherent structures on the wall. The pressure amplitude spectra for x/c=0.73 are presented in Fig. 7. The first thing to note is the very weak effect of the thinner boundary layer on the spectra. The thinner boundary layer flow is characterized by a reduced level of turbulent activity in the range 0.3<F$^+$<2. At reattachment (data not shown), x/c=1.11, the thinner boundary layer flow exhibits higher C_p' at F$^+$>1, while downstream of reattachment, at x/c=1.42, the thinner boundary layer exhibits slightly lower C_p' at F$^+$<0.8. Again, the overall very small effect the thinner boundary layer has on the spectra of the wall C_p' is the main finding here.

3.3 The Effect of Sweep on the Baseline Spectra

It was shown[6] that sweep has two major effects on the model wall pressures: first, the bubble is shorter and second, the level of C_p' from separation to reattachment is higher. Certainly, these two features are

interconnected. The higher level of wall pressure fluctuations is a manifestation of increased turbulence activity, in the form of large coherent structures that mix more effectively across the separated shear-layer, causing earlier reattachment. Fig. 3 presents a comparison between the 2D and 3D wall pressures at M=0.25 and R_c=2.4x10^6 and 4.2x10^6. These data are essentially identical to the high R_c data shown in Fig. 9 of Ref 6. The power spectra for Λ=0 and Λ=30 are compared in Figs. 8a through 8d. The overall level of C_p' immediately downstream of separation (x/c=0.73, Fig. 8a) increases significantly due to sweep. Instead of the single, wide band of C_p' centered on F^+=0.8 in the 2D flow, two peaks can be seen in the 3D flow. A wide and flat ridge, centered on F^+=1, and a very distinct peak centered on F^+=0.3 are evident. It is assumed that the additional peak at F^+=0.3 is due to sweep, and might even be set-up dependent, due to the finite span of the model. The F^+=1 peak scales favorably with the reduced length of the bubble (X_{sp} was maintained as c/2, while it actually is shorter than that of the 2D flow). Above the bubble (i.e. x/c=0.85, Fig. 8b), the F^+=1 peak shifts to lower frequencies while the peak at F^+=0.3 is still present. The spectra of the 2D flow at x/c=0.85 are almost featureless. At reattachment (x/c=1.11, Fig. 8c), the F^+=0.3 peak is still seen for the 3D flow while the overall level of C_p' decreases. The 2D flow shows a sub-harmonic peak at F^+=0.4, while there is no evidence of sub-harmonic resonance in the 3D flow. Downstream of reattachment (x/c=1.42, Fig. 8d) the C_p' spectra for both the 2D and 3D flows decrease over the entire F^+ range, but the decrease for the 3D flow is significantly faster, since x/c=1.42 is further downstream from reattachment for the 3D flow.

4.0 Dynamics of the Controlled Flow
4.1 The Effect of Excitation Frequency in 2D Flow
Fig. 9 presents 2D pressure distributions measured at R_c=4.2x10^6 and M=0.25 with control applied from the x/c=0.64 slot at F^+=0.5 and F^+=1. Even though $<c_\mu>$ at F^+=1 is only a third of $<c_\mu>$ at F^+=0.5, the mean controlled pressures upstream of the slot are identical. A small bubble remains for the controlled flow using F^+=1, while flow separation is delayed using F^+=0.5 with $<c_\mu>$=0.3%. The total rms of the wall pressure fluctuations (C_p') of the F^+=0.5 and F^+=1 controlled flows at x/c=0.67 are identical. While C_p' at F^+=0.5 is amplified up to x/c=0.8, C_p' at F^+=1 saturates at x/c=0.73 and begins to decay rapidly in the smooth pressure recovery region of the flow excited by F^+=1. The mean pressures are identical for x/c>1.1. The approach currently used to determine $<c_\mu>$, is to measure the cavity pressure fluctuations (Fig. 1) and correlate these with the measured velocity fluctuations in the absence of an external stream[1,8]. This procedure allows the evaluation of $<c_\mu>$ over the entire frequency domain of interest, not only at the excitation frequency

and does not rely on the hot-wire de-rectification process that can distort the frequency content. Fig. 10a presents the $<c_\mu>$ for F^+=0.5 and F^+=1 that were calculated from the measured cavity pressure fluctuations. The fundamental excitation frequency contains 81% and 86% of the total excitation momentum for the fundamental of F^+=0.5 and F^+=1 respectively. Note that $<c_\mu>$ of the 2nd harmonic of F^+=0.5 is smaller by an order of magnitude than $<c_\mu>$ of the fundamental of F^+=0.5. The 2nd harmonic of F^+=1 is smaller than the fundamental $<c_\mu>$ by almost three orders of magnitude. Comparing the total fluctuating momentum contained in the fundamental and its higher harmonics, in the range 0.5<F^+<4, indicates that it is 0.38% and 0.14% for F^+=0.5 and F^+=1 respectively, maintaining a ratio of about 3:1 between $<c_\mu>$ of F^+=0.5 and $<c_\mu>$ of F^+=1. Fig. 10b compares the baseline and controlled pressure spectra at x/c=0.73, immediately downstream of the excitation slot and very close to the location of the baseline flow separation. The pressure amplitudes of both excitation frequencies are identical at this location, even though $<c_\mu>$ at F^+=0.5 was three times higher at the excitation slot (Fig. 10a). The C_p' of the 2nd harmonic of F^+=1 is similar to the C_p' of the 3rd harmonic of F^+=0.5. These frequencies generate F^+'s of 1.5 to 2, which were shown to be the most effective frequencies for separation control over this geometry at high Reynolds numbers[1]. It is demonstrated that the flow is most receptive to these F^+'s, because the ratio between excitation momentum and the measured C_p' at these F^+ are the highest. Fig. 10b also shows that the overall level of the pressure fluctuation increases due to excitation, with the exception of F^+<0.1, with respect to the baseline C_p'. The spectra of the wall pressures in the recovery region (x/c=0.85) are presented in Fig. 10c. The most striking feature is the strong decay of the higher harmonics of the excitation at F^+>1, that were very active above the bubble (Fig. 10b). While F^+=0.5 maintains its momentum, F^+=1 decayed between x/c=0.73 and x/c=0.85, and the amplitude of the 2nd harmonic of F^+=0.5 increased. Note that F^+=1 developed two side bands at F^+~0.5 and at F^+~1.5, which is an indication of sub-harmonic resonance. The C_p' downstream of reattachment are presented in Fig.10d. The controlled flow is steadier than the baseline for F^+<0.5, for both excitation frequencies. The decay rate of the F^+=1 related C_p' is faster than the decay rate of F^+=0.5 related C_p'. The random pressure fluctuations of the flow that was excited by F^+=0.5 are lower than the random C_p' of the flow excited by F^+=1. It will be shown later that this feature is related to the excitation level when using low F^+. The C_p' spectra at the end of the measurement domain are presented in Fig. 10e (x/c=1.42). For F^+=1 only the C_p' at the excitation frequency and its 3rd harmonic are higher than the baseline C_p', while for F^+=0.5 the fundamental

and its two higher harmonics rise above the baseline C_p'.

Additional information regarding the dynamics of the control process can be gained by studying the evolution of the excitation related pressure fluctuations $(C_p'_f)$ and the phase speed of the coherent pressure fluctuations. $C_p'_f$ can be extracted from the C_p' spectra for highly coherent flow or from the ensemble averaged pressure fluctuations, phase-locked to the excitation frequency. Fig. 11a compares the $C_p'_f$ at the excitation frequency for the data presented in Figs. 9 and 10. It is demonstrated that the amplitudes at x/c=0.67 are similar even though there was a factor of three in the input excitation momentum. The $C_p'_f$ at $F^+=0.5$ is amplified while at $F^+=1$ the $C_p'_f$ saturates at x/c=0.73. The decay rate of $F^+=1$ is faster than the decay rate of $F^+=0.5$. Similar trends were observed at high R_c (Fig. 14c, Ref. 1). The phase velocities of the coherent wall $C_p'_f$ were calculated using a 3rd order polynomial fit to the evolution of the phase with x/c and normalized by the local velocity at the BL edge, U_e, that was calculated from C_p. The phase velocities above the bubble (Fig. 11b, x/c~0.7) are about $0.3U_e$, close to the linearly expected values for low amplitude disturbances in attached boundary layers, and smaller than those expected in a 2D turbulent mixing layer in the absence of a pressure gradient. The phase velocities increase as reattachment is approached, and the phase velocity of $F^+=1$ accelerates faster. Downstream of reattachment both phase velocities approach 0.8, which is an acceptable value for turbulent boundary layer structures.

The relationship between the fundamental excitation frequency and its second harmonic was evaluated for $F^+=0.5$. Fig. 12a presents the total rms of the wall pressure fluctuations (C_p') as well as the level of $C_p'_f$ at $F^+=0.5$ and at its second harmonic, (i.e. $C_p'_{2f}$, $F^+=1$). Fig. 12b presents the phase velocities of $F^+=0.5$ and its 2nd harmonic. Note that the excitation input is contaminated by higher harmonics since $C_p'_f$ contains only 74% of the total C_p' at x/c=0.67 (it contained 81% of $<c_\mu>$ at the excitation slot, Fig. 10a). The $C_p'_{2f}$ is about 13% of the total C_p' at x/c=0.67, and it initially decays. The phase velocity of the fundamental (Fig. 12b) indicates that it is a convective shear-wave, while the phase velocity of the 2nd harmonic of the excitation frequency indicates that it is initially a standing wave (i.e. $U_\phi \rightarrow 0$). Between x/c=0.77 and x/c=1.25 the phase velocities of F and 2F are similar, within the experimental uncertainty. It is also noted that as F starts to decay, 2F amplifies (Fig. 12a) over the streamwise extent that corresponds to the pressure recovery region (i.e. 0.77<x/c<1, Fig. 9). These findings indicate that a resonant wave interaction is active in the reattachment region. In the attached region of the boundary layer (x/c=1.25), F continues to

accelerate to $0.8U_e$, while 2F, whose amplitude decays slower than the amplitude of F also accelerates slower.

4.2 Excitation Effect in 3D Flow

It was demonstrated[6] that the effectiveness of periodic excitation is not reduced at mild sweep angles. It was further shown that the integral parameters of the controlled 3D flow scale according to simple swept wing scaling[9]. Presently, the dynamics of the 3D controlled flow are examined and several key features of 2D and 3D controlled flows are compared.

Fig. 13 presents baseline and controlled pressure distributions measured at $R_c=4.2\times10^6$, M=0.25 with the model swept to $\Lambda=30$ deg and an excitation slot located at x/c=0.64. The baseline reattachment is assumed at x/c≈1.1 and $X_{sp}=c/2$ is used, for the sake of simplicity and ease of comparison with the 2D flow. The data indicate the effectiveness of $F^+=1$ with $<c_\mu>=0.04\%$ due to the ability of this excitation mode to shorten the separation bubble. C_p' of $F^+=1$ decays immediately downstream of the excitation slot. The flow is less receptive to $F^+=0.5$, as indicated by C_p' of $F^+=0.5$ and $<c_\mu>=0.04\%$ at x/c=0.67 with respect to C_p' of $F^+=1$ at the same $<c_\mu>$. An increase of the excitation momentum of $F^+=0.5$, from $<c_\mu>=0.04\%$ to $<c_\mu>=0.3\%$, results only in a minute increase of C_p' at x/c=0.67. This could be partly due to the effective delay of separation, as indicated by the C_p of $F^+=0.5$, $<c_\mu>=0.3\%$ excited flow. Separation delay, which is the purpose of the control strategy, alters the mean flow and its instability characteristics, making the attached flow less receptive to excitation, leading to saturation of the control effectiveness.

The excitation momentum inputs, at $F^+=0.5$ and $F^+=1.0$ for low $<c_\mu>$ controlled flow data that are presented in Fig. 13, were calculated from the cavity pressure fluctuations and are plotted in Fig. 14a. The values of $<c_\mu>$ at the two fundamental excitation frequencies are identical. The higher harmonics of $F^+=0.5$ (dashed line) are at worst three orders of magnitude smaller than the $<c_\mu>$ of the fundamental. The higher harmonics of $F^+=1$ are about two orders of magnitude smaller than the $<c_\mu>$ of the fundamental, with the 3rd harmonic (i.e. $F^+≈3$) larger than the 2nd harmonic ($F^+=2$). The wall pressure fluctuations spectra at x/c=0.73 are presented in Fig. 14b. The amplitudes of the fundamental are similar, but the comparison is not completely unbiased since the mean flows are different (Fig. 13). The $F^+=0.5$ flow is still separated at x/c=0.73 while the $F^+=1$ excited flow undergoes a pressure recovery. Taking this into account, it can be observed (Fig. 14b) that excited flow at $F^+=0.5$ is dominated by the excitation frequency, while the flow excited at $F^+=1$ shows stronger activity at higher harmonics. Both frequencies eliminated the $F^+=0.3$ mode that was active in the 3D baseline flow.

Fig. 14c presents the baseline and excited flow at x/c=0.85, where both excited flows undergo a pressure recovery. It is interesting to note that 2F for F^+=0.5 is active, along with F, while for F^+=1, 3F is active. Another feature to note is that F^+=1 decays faster than F^+=0.5. This trend also continues at the reattached flow (i.e. x/c=1.11, Fig. 14d and x/c=1.42, Fig. 14e). The 2F of F^+=0.5 and 3F of F^+=1 continue to play a role in the recovery process of the boundary layer downstream of reattachment, with the decay rate of 3F (i.e. F^+=3) being the smallest. Nevertheless, the coherent pressure fluctuations of the F^+=1 excited flow are smaller than those of the F^+=0.5 excited flow.

The effect of increasing the excitation level of F^+=0.5 from $<c_\mu>$=0.04% to $<c_\mu>$=0.3% on the mean and fluctuating wall pressures was also presented in Fig. 13. The total C_p' at x/c=0.67 increased by a very small fraction of the order of magnitude increase in $<c_\mu>$, but the effect on the C_p is significant. To explore this effect, $<c_\mu>$ was calculated (Fig. 15a) for F^+=0.5 at the two excitation levels that were used. The main effect of the increased level of the cavity pressure fluctuations is to increase the magnitude of all spectral peaks by about an order of magnitude, besides the 2nd harmonic that increased almost by two orders of magnitude. The relative magnitude of 3F and 5F (with respect to the logarithmic decay rate as F increases) is larger than 2F and 4F. Fig. 15b presents the wall pressure fluctuations spectra at x/c=0.73. The two mean flows are different (Fig. 13), so the comparison is biased. Still the C_p' of F and 2F are identical, while the high $<c_\mu>$ excitation generated very strong activity at 3F, 4F, 5F and 6F (solid thin line). The level of the random pressure fluctuations was significantly reduced in the high $<c_\mu>$ excited flow (i.e. at frequencies that are not an integer multiple of the excitation frequency).

Fig. 16a presents the amplitudes of the fundamental excitation frequency for the 2D and 3D flows when the flow was excited using F^+=0.5 and $<c_\mu>$=0.3%. The $C_p'_{f,3D}$ amplitude was scaled by $\cos^2(30°)$. The excellent agreement between the 2D and 3D scaled $C_p'_f$ indicate the validity of the conventional 3D scaling for the reattached flow and supports the hypothesis that the wave propagates perpendicular to the excitation slot.

Fig. 16b presents the phase velocities for the F^+=0.5 high $<c_\mu>$ excitation in the 2D and 3D flows. Without any scaling, both phase velocities start with about $0.3U_e$ (x/c≈0.7). The trend of the data is very similar, regardless of the sweep angle, from x/c=0.67 to x/c≈1. For x/c>1, the 2D phase speed accelerates to above 0.8, while the 3D U_ϕ/U_e accelerates to only 0.6, which is too small for large coherent structures in attached turbulent boundary layers. If we assume that the main direction of 3D flow development is along the chord, and scale U_ϕ by $U_e\cos(\Lambda)$ to account for it (Fig.

16b), the agreement between the 2D and 3D scaled phase velocities improves. The agreement is within the experimental uncertainty, from the x/c location of the baseline separation (x/c=0.65) to x/c=1.25.

4.3 The Effect of Steady Suction on the Dynamics of Flow Reattachment

It was shown[1,6] that separation control on the present model could be performed with comparable efficiency using low c_μ steady suction or periodic excitation (i.e. C_μ<0.2%). Furthermore, it was shown that low levels of suction not only shorten the bubble but also increase the level of wall pressure fluctuations under the controlled bubble. Fig. 17a presents a comparison of mean and fluctuating wall pressures measured at high Reynolds number in incompressible 2D flow (R_c=16x10^6, M=0.25, x/c=0.64 slot). It can be seen that the application of steady suction with c_μ=-0.08% shortens the bubble by about 0.2c and moves the $C_p'_{max}$ upstream by a similar distance. Note that a large C_p' was generated at x/c=0.67 due to the suction. To explore the nature of the unsteady effect due to the application of steady suction, the wall pressure spectra were computed along the model and were than normalized by the spectra of the baseline pressure fluctuations in order to enhance the visibility of trends that are related to the control input. The scaled spectra at x/c=0.67 (i.e., immediately downstream of the slot and the baseline separation, Fig. 17b) show two amplified bands of frequencies that were generated by the steady suction. These frequencies are centered on F^+≈1.7 and its 3rd harmonic F^+≈5 (3F). To explore the possibility that the effectiveness of steady suction at these conditions is due to the generation of the unsteady excitation and not directly through thinning of the boundary layer or increasing the shear upstream of separation, excitation with F^+=1.6 and $<c_\mu>$=0.09% is compared to the steady suction in Figs. 17. The mean controlled pressures (Fig. 17a) are similar, with a small exception being the separation at a slightly larger C_p of the suction controlled flow as compared to periodic excitation. For x/c>0.7, both controlled pressure distributions are identical. The fluctuating wall pressures are also similar, with the flow excited at F^+=1.6 having C_p's that are larger by roughly 25% when compared to those generated by steady suction. Both C_p' distributions show a secondary $C_p'_{max}$ at x/c=0.95 that corresponds to reattachment. The spectra of the wall pressure fluctuations (Fig. 17b) of the F^+=1.6 excited flow shows very similar trends to the suction excited flow with three dominant peaks, i.e., those at F and 3F correspond to the most unstable modes of the suction perturbed flow (x/c=0.67). The wall C_p spectra at x/c=1.11 (i.e. downstream of reattachment, Fig. 17b) are very similar for both control methods, reducing the level of the random pressure fluctuations for F^+<1. The flow excited at

$F^+=1.6$ shows the highest relative fluctuations level at 3F, in agreement with the 2D and 3D controlled flow (Figs 10e and 14e). The possibility that the spectral peaks seen for the suction excited flow are generated by a cavity resonance was checked and eliminated. The resemblance between the effects of low C_μ excitation and suction indicates again the possibility of enhancing the control effectiveness by combining periodic excitation and steady suction for separation control[1,10].

5. Conclusions

The dynamics of active control of flow separation on a Glauert-Goldschmied type aerodynamic surface were investigated experimentally. Most of the results presented in this paper are for lower Reynolds numbers than those included in two previous publications, but the effect of the Reynolds number on the flow was shown to be small due to the inviscid nature of the curvature induced separation.

Evidence was found for the existence of a sub-harmonic resonance in the baseline 2D separated shear-layer. A reduction of 35% in the momentum thickness of the upstream boundary layer has a negligible effect on the mean and fluctuating wall pressures and only a weak effect on the pressure spectra. It is speculated that flow separation on the present model is caused mainly by the local curvature rather than by adverse pressure gradient or viscous effects. The level of the wall pressure fluctuations in the 3D separated flow is significantly higher than in its 2D counterpart. This is a manifestation of the additional 3D streamwise vorticity that can roll-up to generate discrete unsteady streamwise vortices superposed on the spanwise vortices. Regardless of the mechanism, the result is shortening of the 3D separated flow region. Controlled 2D data shows that the separated shear layer is most receptive to $F^+=1.5$ to 2 and also amplifies these F^+'s. Non-linear wave resonance between $F^+=0.5$ and $F^+=1$ plays an important part in the reattachment process. Downstream of reattachment the low F^+'s decay, with the decay rate of 3F being the slowest. It was demonstrated that the increased efficacy of low F^+, high $<c_\mu>$ excitation is through generation of higher harmonics and non-linear interaction among the several excited waves. The swept flow separation is more receptive to $F^+=1$ excitation than its 2D counterpart, and also reduces the random pressure fluctuations more effectively. High-level excitation generates stronger coherent wave motion at higher F^+, and controls the random motion more effectively. Conventional swept wing scaling works well also for the phase locked pressure wave features.

The effect of weak steady suction is to promote wide band unsteady excitation that evolves in a similar manner to the evolution of coherent excitation at $F^+=1.6$. The most unstable frequency bands for separation control on the present geometry are $F^+\sim1.5$ and $F^+\sim5$.

References

1. Seifert, A. and Pack, L.G., "Active Control of Separated Flows on Generic Configurations at High Reynolds Numbers (Invited)", AIAA paper 99-3403, 30th AIAA Fluid Dynamics Conference, Norfolk, VA, June 1999.
2. Mabey, D.G., "Analysis and correlation of data on pressure fluctuations in separated flow", Journal of Aircraft, Vol 9, Sept. 1972, pp. 642-645.
3. Rokwell, D., "Oscillations of Impinging Shear Layers", AIAA J., Vol. 21, No. 5, May 1983, pp. 645-664.
4. Le, H., Moin, P. and Kim, J., "Direct Numerical Simulation of Turbulent Flow over a Backward-facing Step, Journal of Fluid Mechanics, Vol. 330, 1997, pp. 349-374.
5. Na, Y. and Moin, P., "Direct Numerical Simulation of a separated turbulent boundary layer, JFM, Vol. 374, 1998, pp. 379-405.
6. A. Seifert and L.G. Pack, "Sweep & Compressibility Effects on Separation Control at High Re Numbers", AIAA paper 2000-0410,
7. Glauert, M. B., "The Design of Suction Aerofoils with a Very Large C_l-Range", Aeronautical Research Council, R.&M. 2111, November 1945.
8. Seifert, A. and Pack, L.G., "Oscillatory Control of Separation at High Reynolds Numbers", AIAA J., Vol. 37, No. 9, Sep. 1999, pp. 1063-1071.
9. Naveh, T., Seifert, A., Tumin, A., and Wygnanski, I., "Sweep Effect on Parameters Governing Control of Separation by Periodic Excitation", Journal of Aircraft, Vol. 35, No. 3, 1998, pp. 510-512.
10. Greenblatt, D., Nishri, B., Darabi, A. and Wygnanski, I., "Some Factors Affecting Stall Control with Particular Emphasis on Dynamic Stall, AIAA paper 99-3504, Norfolk, VA June 28-July1, 1999.
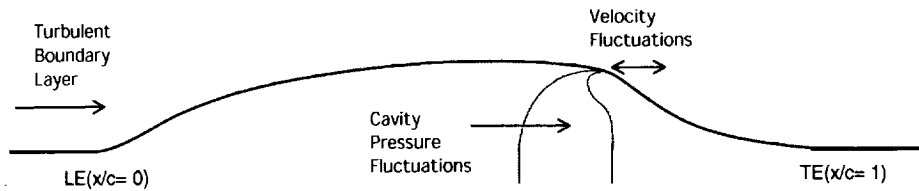
Fig. 1 Cross section of the wind tunnel model, with an excitation slot at x/c=0.64, as mounted on the tunnel sidewall.
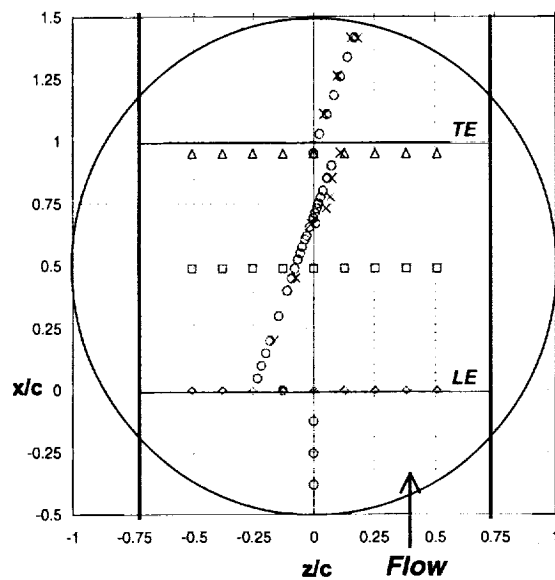

Fig. 2 Top view of the 2D model. The thick vertical lines indicate the location of the end plates and the x symbols indicate the location of the unsteady pressure transducers.
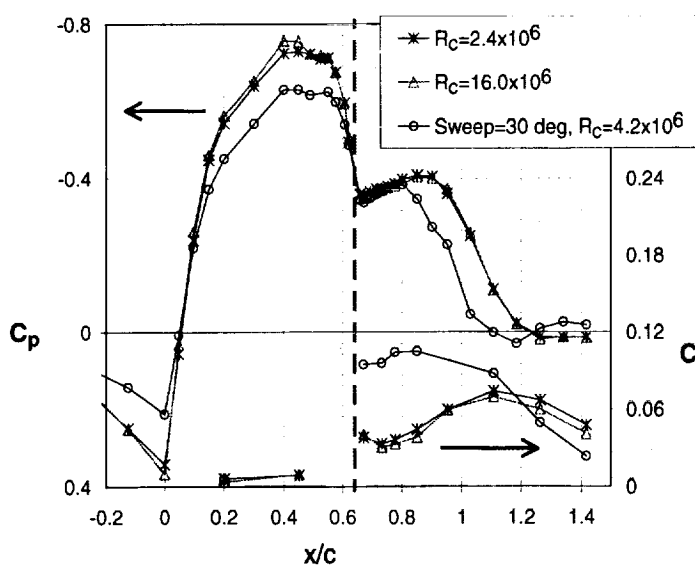

Fig. 3 Mean and fluctuating wall pressures of the baseline 2D and 3D flow, R_c = 2.4 and 16x10^6, M=0.25, slot x/c=0.64.
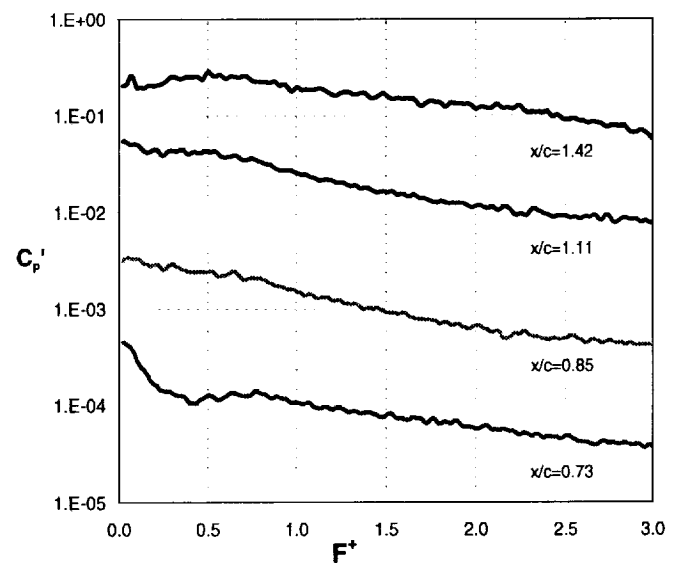

Fig. 4 Spectra of the wall pressure fluctuations, 2D baseline flow, R_c = 4.2x10^6, M=0.25, slot x/c=0.64..

American Institute of Aeronautics and Astronautics
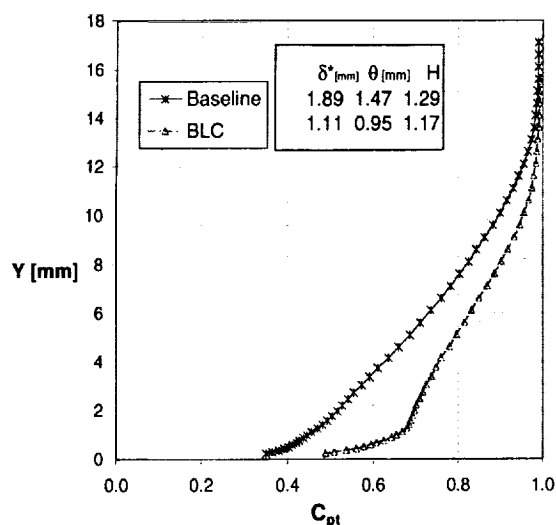
Fig. 5 Boundary layer total pressure profiles measured 1.25c upstream of the LE with and without boundary layer thinning, $R_c = 4.2 \times 10^6$, M=0.25.
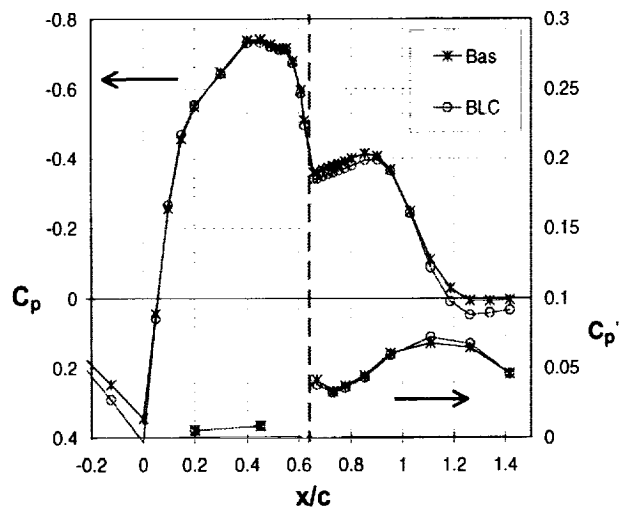
Fig. 6 Mean and fluctuating baseline wall C_p's, conditions of Fig. 5.
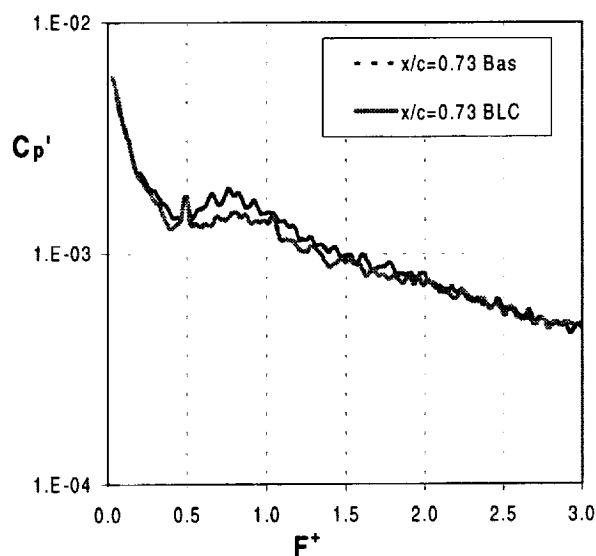
Fig. 7 Spectra of the wall pressure fluctuations measured at x/c=0.73, 2D baseline flow, with and without boundary layer thinning, $R_c = 4.2 \times 10^6$, M=0.25.
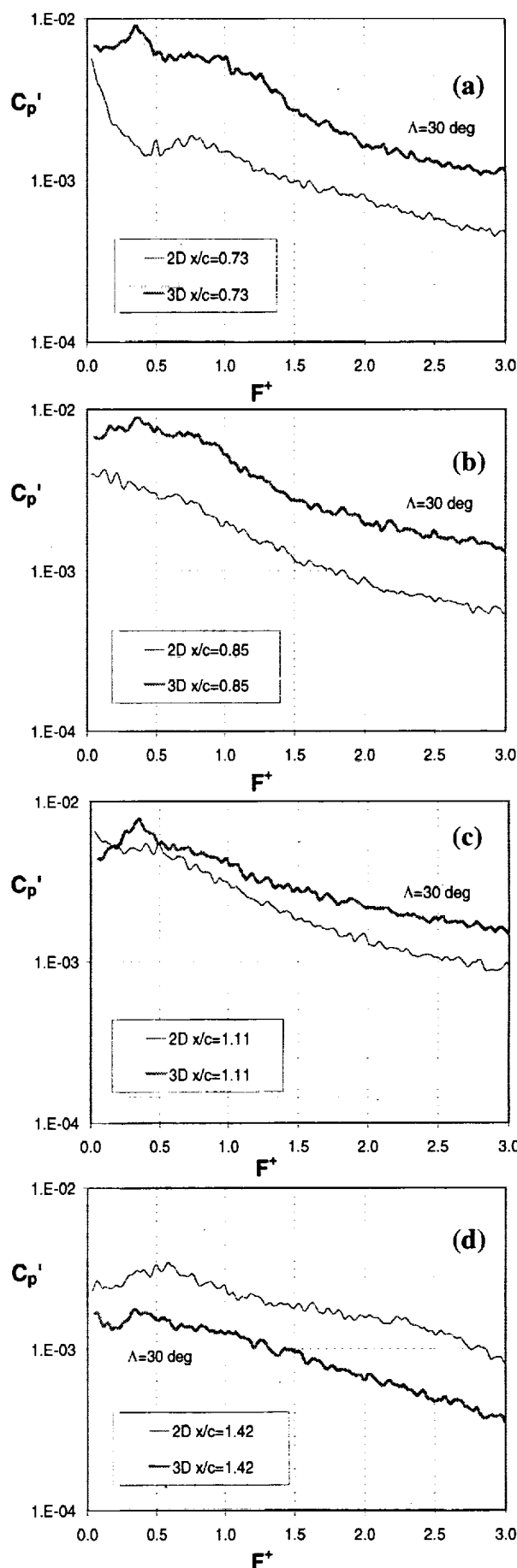
Fig. 8a-d Spectra of the wall pressure fluctuations for 2D and swept (3D) flows measured at x/c=0.73 (a), x/c=0.85 (b), x/c=1.11 (c) and x/c=1.42 (d). $R_c = 4.2 \times 10^6$, M=0.25.

10
American Institute of Aeronautics and Astronautics
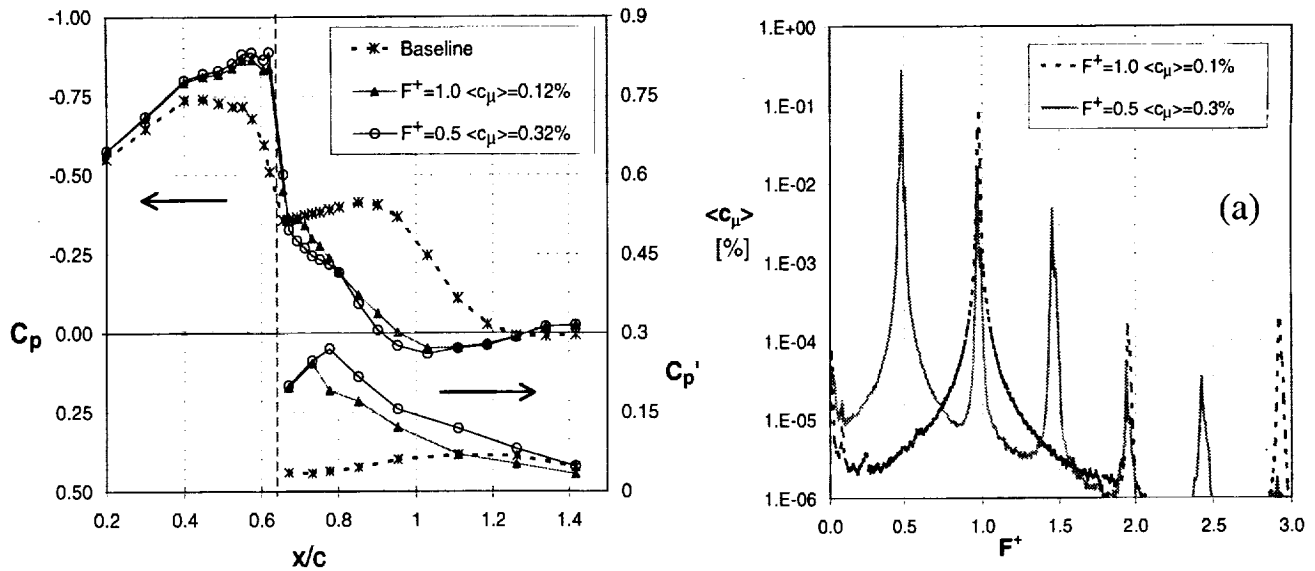
Fig 9 Mean and fluctuating wall pressures of the baseline and controlled 2D flow, $R_c = 4.2 \times 10^6$, M=0.25, slot x/c=0.64.
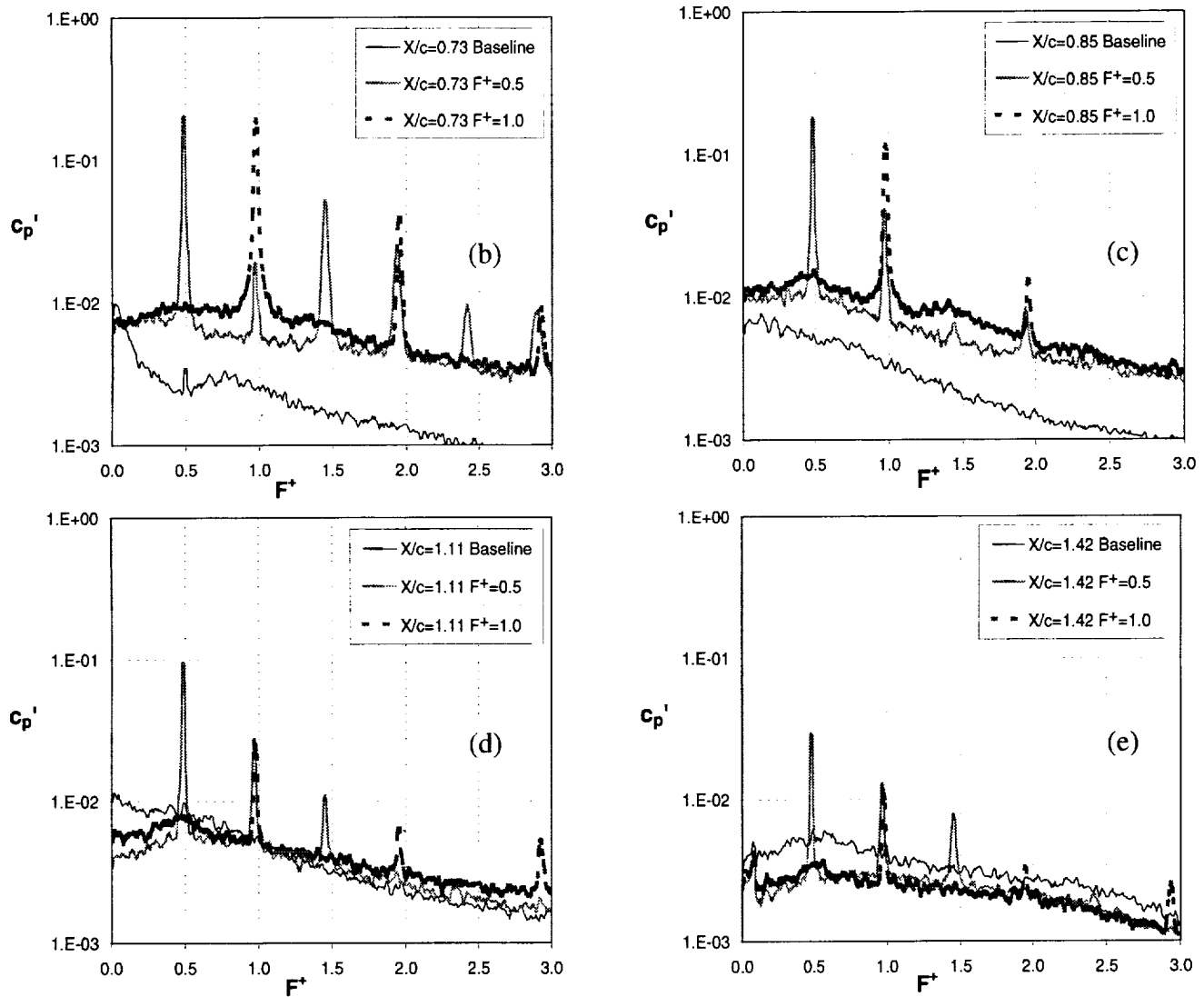
Fig 10 Spectra of $<c\mu>$ input (a), and wall pressure fluctuation for 2D baseline and controlled flows measured at x/c=0.73 (a), x/c=0.85 (b), x/c=1.11 (c) and x/c=1.42 (d). $R_c = 4.2 \times 10^6$, M=0.25, slot x/c=0.64.
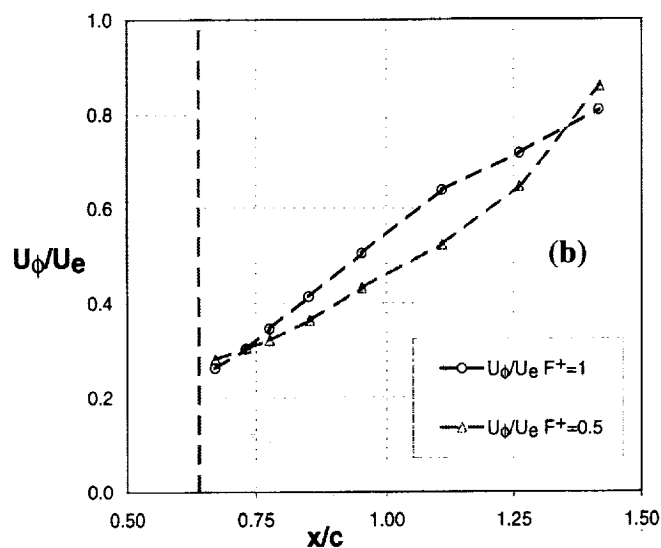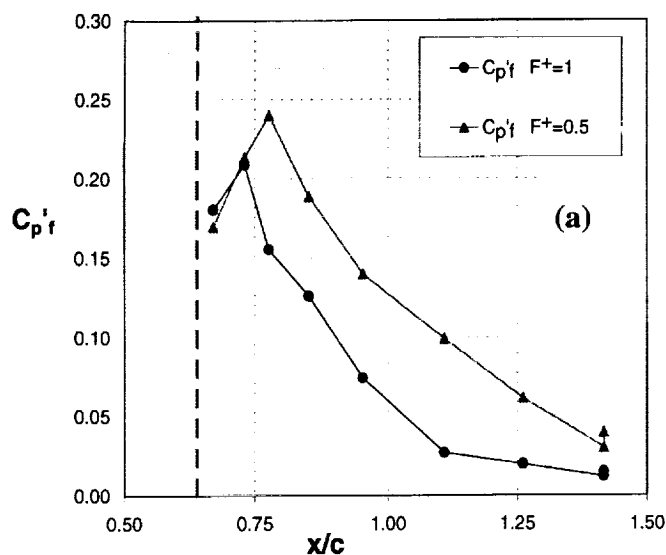
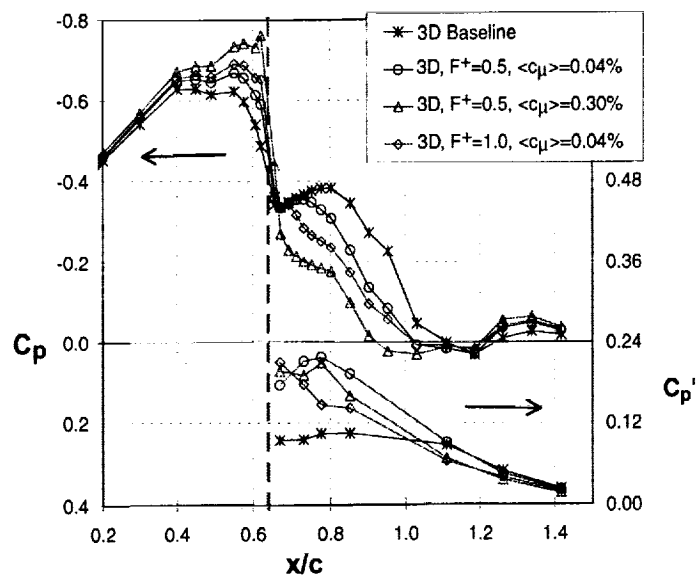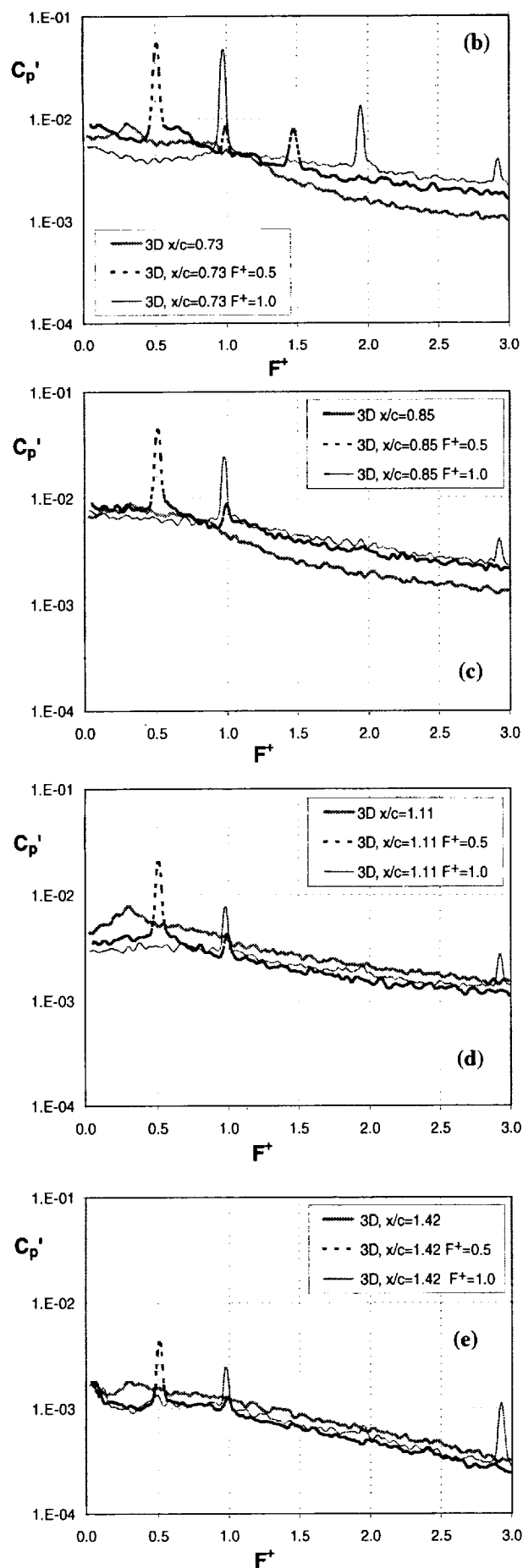**Fig 11** C_p' phase locked to the excitation frequency (a), and phase velocity (b). Conditions as in Figs. 9 and 10.
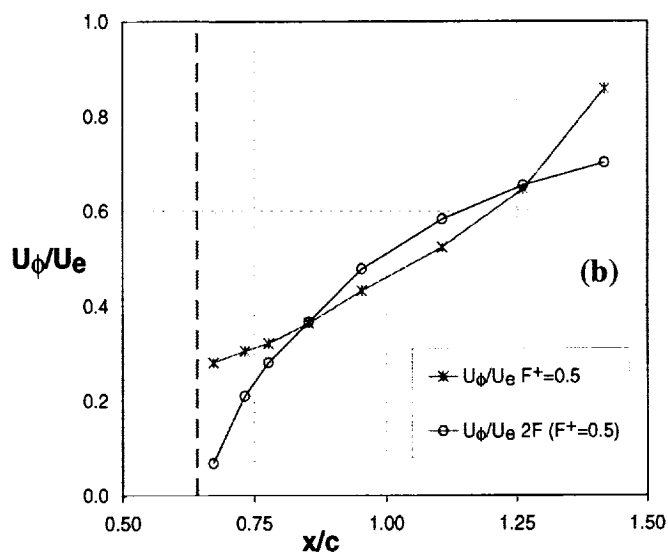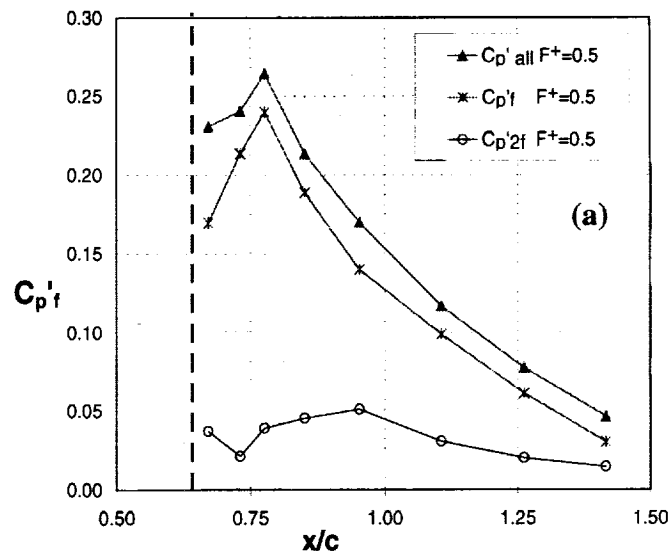
Fig 12 Total and phase locked C_p' at the fundamental excitation frequency and its second harmonic (a), and phase velocities (b). F^+=0.5, $<c_\mu>$ =0.32%, R_c = 4.2x10^6, M=0.25, slot x/c=0.64.

Fig 13 Mean and fluctuating wall pressures of the baseline and controlled 3D flow, R_c = 4.2x10^6, M=0.25, slot x/c=0.64.
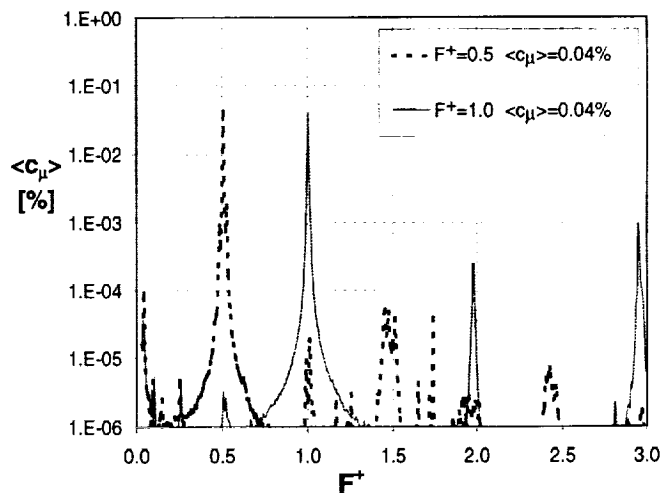
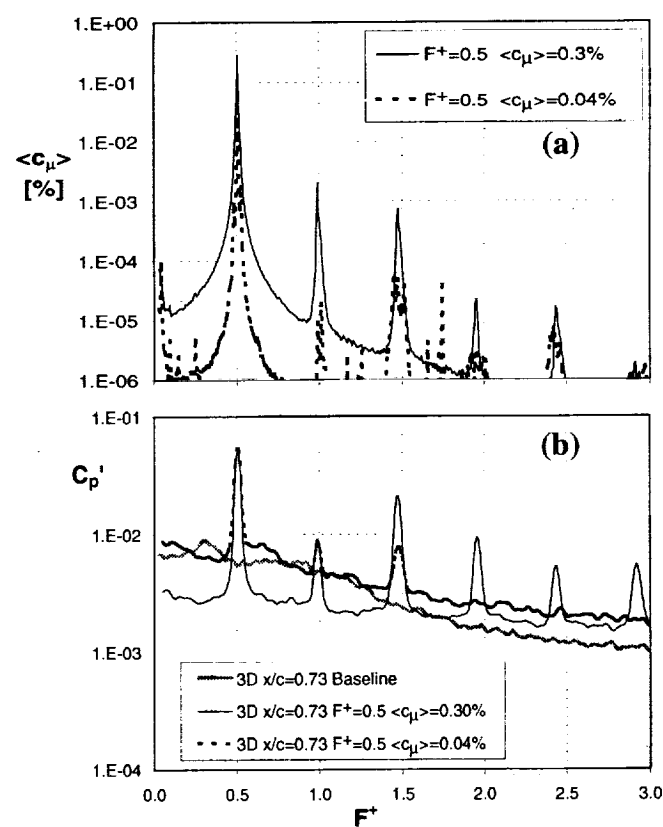**Fig 14a** Spectra of $<c_\mu>$ input, R_c = 4.2x10^6, M=0.25, slot x/c=0.64, F^+ indicated in legend.

Fig 15 Spectra of $<c_\mu>$ input (a), and wall pressure fluctuations for 3D baseline and controlled flows measured at x/c=0.73 (b). $R_c = 4.2 \times 10^6$, M=0.25, slot x/c=0.64, F^+=0.5, $<c_\mu>$ indicated in legend.

Fig 14 Spectra of the wall pressure fluctuations for 3D baseline and controlled flows measured at x/c=0.73 (b), x/c=0.85 (c), x/c=1.11 (d) and x/c=1.42 (e). $R_c = 4.2 \times 10^6$, M=0.25, slot x/c=0.64, $<c_\mu>$=0.04%, F^+ indicated in legend.
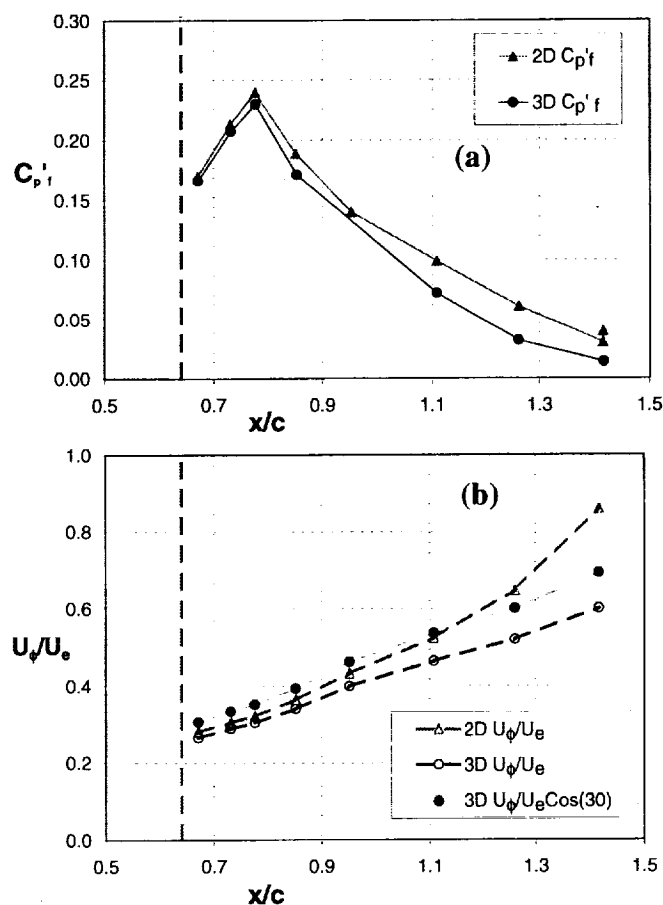
Fig 16 Phase locked C_p' at the fundamental excitation frequency (a), and phase velocities (b) for 2D and 3D flows. F^+=0.5, $<c_\mu>$ ≈0.3%, $R_c = 4.2 \times 10^6$, M=0.25, slot x/c=0.64.
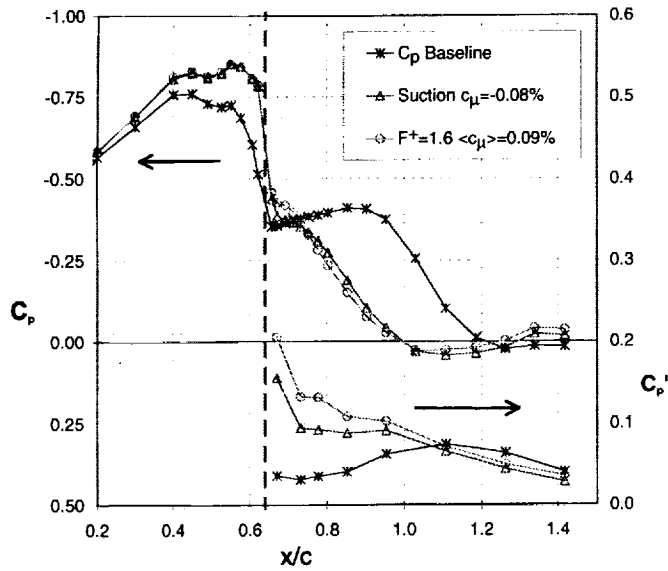
Fig 17a Mean and fluctuating wall pressures of the baseline and controlled 2D flow using suction or periodic excitation, $R_c = 16 \times 10^6$, M=0.25, slot x/c=0.64.
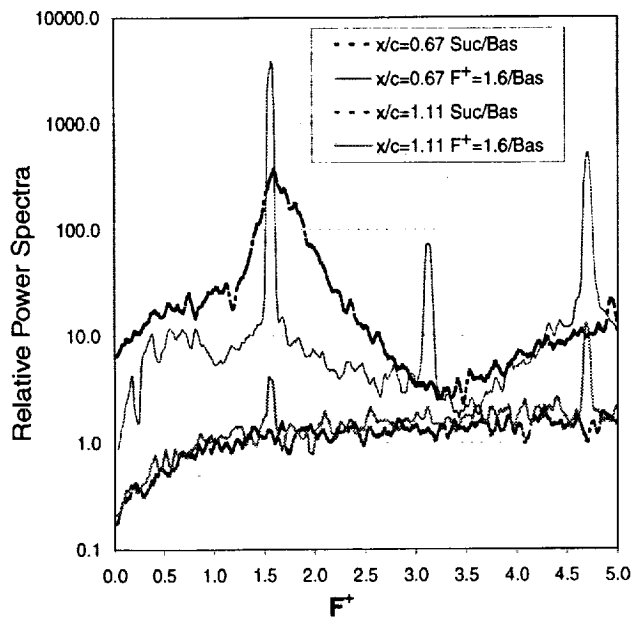

Fig 17b Wall pressures spectra of the controlled 2D flow normalized by the baseline spectra. Same conditions as the data of Fig. 17a.

American Institute of Aeronautics and Astronautics